
[View Journal Online](#)
[View Article Online](#)

Crystal growth and some physicochemical studies on an organic intermolecular compound of anthranilic acid and *N,N*-dimethylamino benzaldehyde

 Uma Shanker Rai ^{1,*}, Manjeet Singh ² and Rama Nand Rai ¹
¹ Department of Chemistry, Centre of Advanced Study, Institute of Science, Banaras Hindu University, Varanasi-221005, India
usr_1_bhu@yahoo.co.in (U.S.R.), rn_rai@yahoo.co.in (R.N.R.)

² Crystallography and Crystal Chemistry Laboratory, Department of Chemistry, Indian Institute of Science Education and Research Bhopal, Bhopal By-Pass Road, Bhuri, Bhopal-462066, Madhya Pradesh, India
manjeet@iiserb.ac.in (M.S.)

 * Corresponding author at: Department of Chemistry, Centre of Advanced Study, Institute of Science, Banaras Hindu University, Varanasi-221005, India.
 Tel: +91.542.6701605 Fax: +91.542.2368127 e-mail: usr_1_bhu@yahoo.co.in (U.S. Rai).

RESEARCH ARTICLE

ABSTRACT



doi 10.5155/eurjchem.9.4.303-310.1720

 Received: 21 April 2018
 Received in revised form: 01 June 2018
 Accepted: 02 June 2018
 Published online: 31 December 2018
 Printed: 31 December 2018

The phase diagram of anthranilic acid and *N,N*-dimethylaminobenzaldehyde system gives two eutectics (E_1 and E_2) and a 1:1 intermolecular compound with congruent melting point. The mole fractions of anthranilic acid at E_1 and E_2 are 0.10 and 0.95, respectively. The negative values of heat of mixing of eutectics suggest that there is clustering of molecules in their eutectic liquid melt. The positive values of excess free energy for eutectics indicate that the interactions between the like molecules are stronger than those of unlike molecules. It can be inferred from single crystal X-ray analysis of the intermolecular compound that it crystallized in monoclinic unit cell with $C2/c$ space group and a reasonably large sized intermolecular compound crystal was grown by slow evaporation technique at room temperature. The optical studies on the intermolecular compound give two strong emission bands with two λ_{max} values one at 380 nm and second at 450 nm with total quantum efficiency 0.49.

KEYWORDS

 Emission
 Heat of fusion
 Phase diagram
 Crystal growth
 Intermolecular interaction
 Single crystal X-ray analysis

 Cite this: *Eur. J. Chem.* 2018, 9(4), 303-310

 Journal website: www.eurjchem.com

1. Introduction

It is well known that the green synthesis which utilizes the starting materials most efficiently to give maximum yield has become a potential alternative route to produce novel materials of technical and potential importance [1-5]. During the last three decades, organic molecules are widely exploited to engineer the molecules for non-linear optics (NLO), organic conductors, ferromagnetic materials, optical sensors, charge transfer complexes and supra-molecular device applications, among others. The wider choice of organic compounds along with possibility in variation of their properties as a result of various functional groups on different positions in the molecules, have opened potential opportunities to produce numerous organic materials to cater the needs of modern civilization [6,7]. Binary organic compounds are being exploited for their promising properties such as light emitting diodes of variable colors including white light, nonlinear optical, electro-optic and conducting materials. Recently, the studies on binary organic materials have been extended to

produce the nonlinear optics and white light emitting diode (WLED) [8,9].

In the anthranilic acid (AA) and *N,N*-dimethylamino benzaldehyde (DMAB) system, the values of enthalpy of fusion of the former is 24.59 kJ/mol and that of the latter is 20.03 kJ/mol. These high values suggest that the system is an organic analogue of nonmetal-nonmetal system. The presence of electron rich amino group and that of electron deficient carbonyl group shows high possibility of formation of intermolecular compounds. To identify the composition and melting points of the binary materials (Eutectics and intermolecular compound (IMC)) the phase diagram of the system was determined. Convenient amount of these materials was prepared by the solvent free green synthesis involving molten state reactions. They were characterized by the differential scanning calorimetry (DSC), powder X-ray diffraction, Fourier transform-infrared (FT-IR) spectroscopy and nuclear magnetic resonance (NMR). Single crystal of the IMC was grown and its crystal analysis, atomic packing was also studied along with optical properties.

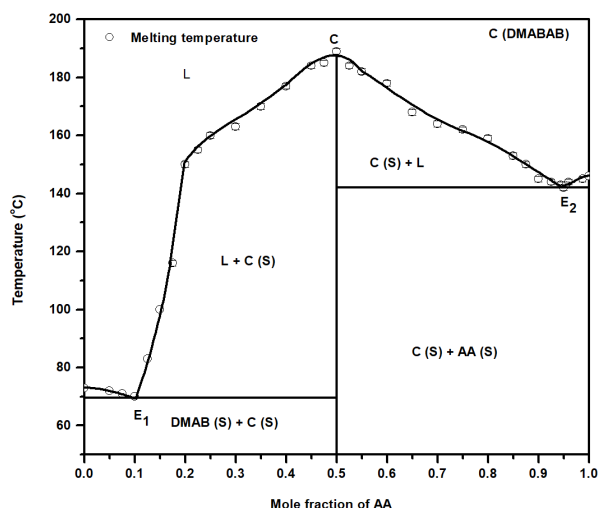


Figure 1. Phase diagram of AA and DMAB system.

2. Experimental

2.1. Materials and their purification

Both parent compounds, namely, anthranilic acid (99%) and *N,N*-dimethylaminobenzaldehyde (99%) were obtained from Aldrich, Germany and they were purified by repeated crystallization from ethyl acetate. The purity of each of the compounds was ascertained by comparing the experimental melting temperatures of AA and DMAB, 148.0 and 74.0 °C, respectively, with their melting temperatures provided in the literature [10].

2.2. Phase diagram

The phase diagram of AA-DMAB system was determined by the thaw-melt method [11] in the form of temperature-composition curve. In this method, mixtures of two components, covering the entire range of compositions, were prepared and they were homogenized four times by their melting followed by chilling in ice cooled water. The melting temperature of each composition was recorded using a melting point apparatus (Toshniwal) attached with a precision thermometer with an accuracy of ± 0.5 °C.

2.3. Enthalpy of fusion

The values of heat of fusion of the pure components, the eutectics and the intermolecular compound were determined [12] by DSC (Mettler DSC-4000). Indium and zinc samples were used to calibrate the DSC unit. The amount of test sample and heating rate were about 7 mg and 5 °C/min, respectively.

2.4. Spectroscopic studies

Infrared spectra of the pure components and the intermolecular compound were recorded at 300 K in the region 4000- 400 cm^{-1} using a Perkin Elmer FT-IR Spectrum 1000 infrared spectrometer. The NMR spectra were recorded in CDCl_3 by JOEL 300 MHz spectrometer.

2.5. X-ray diffraction

Powder X-ray diffraction (XRD) patterns for pure components, eutectics and IMC were recorded using an 18 kW rotating (Cu) anode based Rigaku powder diffractometer fitted

with a graphite monochromator in the diffracted beam. The samples were scanned from 10 to 70 ° with a scanning rate of 4 °/min.

2.6. Single crystal growth and study of atomic packing

The single crystal of the IMC was grown in a saturated solution of methanol at room temperature by slow vaporization technique. X-ray diffraction data of the single crystal were collected using the Xcalibur Oxford CCD diffractometer. The data reduction was carried out using APEX2 [13]. Structure solution and refinement were carried out utilizing SHELXS and SHELXL-97 [14].

2.7. Optical characterization

The absorption spectra of all starting compounds and IMCs were recorded using UV/Vis/NIR (JASCO model V-670) spectrometer from 190 to 700 nm at room temperature in methanol solution (1.0×10^{-5} M). Fluorescence spectra were also recorded on a Varian Cary Eclipse Fluorescence spectrophotometer using Pyrene as reference at room temperature in the same solvent and concentration.

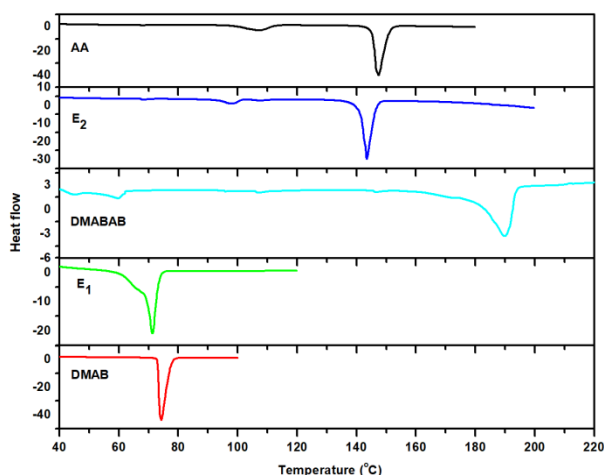
3. Result and discussion

3.1. Phase diagram

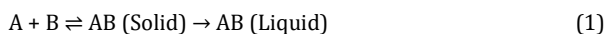
The phase diagram of the AA-DMAB system shows the formation of a 1:1 intermolecular compound (DMABAB) having congruent melting point and two eutectics E_1 and E_2 containing 0.10 and 0.95, mole fractions of AA, respectively. The melting points of E_1 , E_2 and the intermolecular compound are 68.0, 143.0 and 187.0 °C, respectively (Figure 1). It is obvious from Figure 1 that the melting point of DMAB decreases with the addition of the second component AA and it attains the minimum value at the first eutectic point E_1 because up to the eutectic composition AA behaves just like impurity in DMAB. Further addition of the second component causes the melting point to rise till it attains the maximum at C where the compositions of liquid and solid phases are identical. This maximum temperature is the congruent melting point of the IMC. Further increase in mole fraction of the second component causes the melting point of the mixture to decrease and it attains the minimum at the second eutectic point E_2 .

Table 1. Enthalpy of fusion, heat of mixing, entropy of fusion, roughness parameters and interfacial energy of pure components, their eutectics and inter-molecular compound.

S.N.	Materials	Enthalpy of fusion (kJ/mol)	Heat of mixing (kJ/mol)	Entropy of fusion (J/mol.K)	Roughness parameter (α)	Interfacial energy (erg/cm ²)
1	AA	24.59	-	58.5	7.04	47.96
2	DMAB	20.03	-	57.7	6.94	31.45
3	Eutectic 1	(Exp.) 20.63 (Cal.) 20.27	-0.36	60.0	7.22	30.84
4	Eutectic 2	(Exp.) 24.09 (Cal.) 24.26	-0.17	57.9	6.96	46.00
5	DMABAB	(Exp.) 21.24 (Cal.) 22.31	-1.07	45.9	5.52	28.42

**Figure 2.** DSC plots of AA, DMAB, their eutectics and inter-molecular compound.

The existence of a maximum and eutectic points on either side of the maximum point impart stability [15] to the DMABAB. The reaction between two components could be represented by equation:



However, when dissociation occurs in the molten state, the products of dissociation lower the effective mole fraction of the solute, and the curve would be flattened. For each eutectic, the DMABAB behaves as one of the components. The observed maximum in the system under investigation is sharp indicating that the DMABAB is capable of existing in solid form in equilibrium with a liquid of the same composition.

3.2. Enthalpy of fusion

The idea about the structure of eutectic melt and the nature of interaction between the two components forming the eutectic and the addition compound could be obtained from the knowledge of their enthalpy of fusion data. The differential scanning calorimetry plots are shown in Figure 2. The experimental values of enthalpy of fusion and the values that are computed using the mixture law [16] in case of binary materials are included in Table 1. The value of enthalpy of mixing which is the difference between the experimental and the calculated values of heat of fusion is negative suggesting thereby a clustering of molecules for both binary eutectic melt [17,18]. The entropy of fusion ($\Delta_{\text{fus}}S$) of the pure components, the eutectic and IMC can be calculated using the Equation (2),

$$\Delta_{\text{fus}}S = \frac{\Delta_{\text{fus}}H}{T} \quad (2)$$

where T is the melting temperature of the compound. The values of the entropy of fusion (Table 1) being positive suggest that there is increase in randomness of the system during

melting as expected. The enthalpy of fusion value also influences the critical radius and interfacial energy. When a melt is cooled below its equilibrium melting temperature, the liquid phase does not solidify spontaneously because, under equilibrium condition, it contains a number of clusters of molecules. So long as the clusters are all below the critical size [19], they cannot grow to form crystals and, therefore, no solid would result.

The interfacial energy (σ) is related to the critical size (r^*) of the nucleus according to the Equation (3),

$$r^* = \frac{2\sigma T_{\text{fus}}}{\Delta_{\text{fus}}H \Delta T} \quad (3)$$

where, T_{fus} , $\Delta_{\text{fus}}H$ and ΔT are melting temperature of eutectic, heat of fusion and degree of under-cooling, respectively. The interfacial energy is given by the expression,

$$\sigma = \frac{C \Delta_{\text{fus}}H}{(N_A)^{1/3} (V_m)^{2/3}} \quad (4)$$

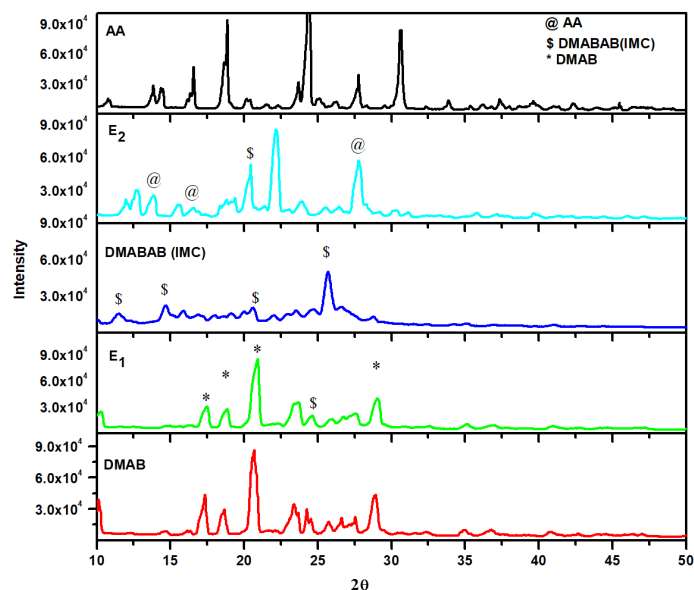
where, N_A is the Avogadro Number, V_m is the molar volume, and parameter C lies between 0.30 to 0.35. The values of interfacial energy of pure components and eutectics, calculated by using the enthalpy of fusion data are also reported in Table 1. The value of σ being the maximum in case of AA and the minimum in that of the IMC suggests that the maximum free energy in case of AA and minimum free energy in case of the IMC are required for the crystallization process to set in.

3.3. Excess thermodynamic functions

A measure of deviation from ideal behavior can be best expressed in terms of excess thermodynamic functions, namely, excess free energy (g^E), excess enthalpy (h^E), and excess entropy (s^E) which give a more quantitative idea about

Table 2. Excess thermodynamic functions of eutectics of the AA-DMAB systems.

S.N.	Systems	g^E (kJ/mol)	h^E (kJ/mol)	s^E (kJ/mol.K)
1	Eutectic 1	0.2013	8.4020	0.0238
2	Eutectic 2	0.4624	-1.8704	0.0056

**Figure 3.** Powder X-ray diffraction pattern of AA, DMAB, their eutectics and IMC.

the nature of molecular interactions. The excess thermodynamic functions (Y^E) is defined as the difference between the thermodynamic functions of mixing for a real system and the corresponding values for an ideal system at the same temperature and pressure.

$$Y^E = \Delta Y_{\text{mix}}(\text{real}) - \Delta Y_{\text{mix}}(\text{ideal}) \quad (5)$$

where Y is any of the excess thermodynamic functions. The excess thermodynamic functions could be calculated using the equations reported earlier [18,20,21] and the values are given in Table 2. The positive values of excess free energy for both eutectic (E_1 and E_2) indicate that the interaction between the like molecules (DMAB-DMAB, DMABAB-DMABAB and AA-AA) are stronger than the interaction between the unlike molecule (DMAB-DMABAB and DMABAB-AA) [18,20,21].

3.4. Spectroscopic studies

In AA-DMAB system, the peaks observed at 3325, 3240, 1677 and 1662 cm^{-1} in the spectrum of AA are due to N-H, O-H and C=O stretching frequency of amine (NH_2), hydroxyl and carbonyl of carboxylic groups, respectively. In the ^1H NMR spectrum of AA the peaks appear at δ 6.67 ppm (4H, d, Ar-H), 7.32 (2H, s, NH_2) and 7.94 ppm (1H, s, OH). In the spectrum of DMAB, the peaks observed at 2795, 2713, and 1662 cm^{-1} are due to C=O stretching frequency of carbonyl of aldehyde groups. In the ^1H NMR spectrum of DMAB peaks appear at δ 9.87 (1H, s, OH), 7.63 (2H, d, Ar-H), 6.78 (2H, d, Ar-H) and 2.85 ppm (6H, s, CH_3). The peaks observed at 3434, 2922, 1677 and 1587 cm^{-1} in the spectrum of their IMC are due to O-H, N-H, C=O stretching frequency of carboxylic and imine groups ($-\text{C}=\text{N}-$), respectively. In the ^1H NMR spectrum of IMC peaks appear at δ 3.11 (6H, s, CH_3), 8.52 (1H, s, NH), 8.33 (1H, d, Ar-H), 7.77 (1H, t, Ar-H), 7.55 (1H, t, Ar-H), 7.44 (1H, d, Ar-H), 7.33 (2H, d, Ar-H), 6.77 (2H, d, Ar-H) and 9.67 ppm (1H, s, OH). The new peak at 8.52 ppm in NMR spectrum and the changes in the intensity and position of IR peaks of the components in

the IMC suggest that there is formation of an inter-molecular compound due to hydrogen bonding between the two components.

3.5. Powder X-ray diffraction studies

Powder X-ray diffraction patterns of parent compounds, their eutectics and inter-molecular compound are recorded and depicted in Figure 3. It is evident from the figure that the XRD pattern of the inter-molecular compound shows some new peaks which could not be assigned for either of parent components, and the change in the intensity of some of the parent peaks confirms the formation of a new compound [22]. While the powder XRD pattern of the eutectic E_1 shows almost all the peaks of the AA compound and some peaks of the IMC whereas the eutectic E_2 powder XRD pattern shows the peaks of the IMC and DMAB confirming thereby that at the point eutectic E_1 weak interactions exist between DMAB and the IMC and at eutectic E_2 between IMC and AA. For eutectic E_1 the peak of AA and for eutectic E_2 the peaks of DMAB could not be assigned, rather we could assign the peaks of the IMC in both eutectics from which it can be inferred that the IMC behaves as a parent component for both the eutectics.

3.6. Crystal growth

The solubility measurement of a material in any solvent gives idea about the nucleation temperature and availability of the solute material for crystal growth as well as to decide the cooling rate during the crystal growth. Super saturation is the driving force for the crystal growth and it also influences the crystal quality [23]. The conditions for the crystal growth of IMC were optimized for methanol and a 100 mL saturated solution was prepared at 43.0 $^\circ\text{C}$ which was kept for slow evaporation of solvent at room temperature. A large sized IMC was grown in three weeks, which are shown in Figure 4. The sharp edges and transparency of the crystal are apparent from the photograph of the crystal in Figure 4.

Table 3. Crystal data and details of the refinement for the IMC.

Parameter	Value
Formula	C ₁₆ H ₁₆ N ₂ O ₂
<i>M_r</i>	268.31
CCDC No.	940623
Crystal system	Monoclinic
Space group	C2/c
<i>a</i> (Å)	18.167(3)
<i>b</i> (Å)	13.0454(8)
<i>c</i> (Å)	15.377(3)
β (°)	129.65(3)
<i>V</i> (Å ³)	2805.9(14)
<i>Z</i>	8
<i>D</i> _{calcd} (g cm ⁻³)	1.270
μ(MoK _α) (mm ⁻¹)	0.085
<i>F</i> (000)	1136
<i>h, k, l</i> range	-24/23, -17/16, -21/20
<i>T</i> (K)	293
Reflections measured	3804
Reflections unique	3077
Data with <i>F</i> _o > 4σ(<i>F</i> _o)	1651
<i>R</i> _{int}	0.0215
Parameters refined	185
<i>R</i> (<i>F</i>) (for <i>F</i> _o > 4σ(<i>F</i> _o))	0.0529
<i>wR</i> (<i>F</i> ₂) (all reflections)	0.1423
GoF (<i>F</i> ₂)	1.024

Table 4. List of intermolecular interactions in the IMC.

Interactions	Symmetry	Geometry		
		D...A (Å)	H...A (Å)	D-H...A (°)
O1-H15...N2	x, y, z	2.510	1.642	152
C7-H7...O1	x, y, z	3.787	2.835	147
C13-H13...O7	x+1/2,-y+1/2+1,+z+1/2	3.485	2.679	131
C2-H1A...N2	x-1/2,-y+1/2+1,+z-1/2	3.490	2.686	117
C2-H2B...N1	-x-1/2,-y+1/2+1,-z	3.689	2.865	133
C9-H9...O2	-x+1/2,+y-1/2,-z+1/2	3.636	2.561	173
C11-H11...O1	-x+1/2,+y-1/2,-z+1/2	3.610	2.812	131
C11-H11...O2	-x+1/2,+y-1/2,-z+1/2	3.605	2.572	160
C4-H4...O2	x-1/2,+y-1/2,+z	3.221	2.228	152

**Figure 4.** Photograph of the single crystal of IMC.

3.7. Single crystal X-ray diffraction

The single crystal of the inter-molecular compound was grown from the saturated solution of methanol using slow evaporation technique at room temperature. A transparent single crystal was selected for X-ray diffraction and analysis. From the single crystal X-ray diffraction analysis of crystal it can be inferred that it has been crystallized in monoclinic unit cell with C2/c space group (CCDC No. 940623) with one molecule in asymmetric unit. The lattice parameters as well as various other crystallographic data of the IMC are given in Table 3 and all relevant intermolecular interactions are tabulated in Table 4. The selected bond angle and bond length between different atoms of IMC are given in Table 5. The ORTEP view and numbering scheme of the IMC are shown in Figure 5a, and its unit cell diagram is given in Figure 5b. The three dimensional packing of IMC is stabilized via mainly O-H...O, C-H...O and C-H...N hydrogen bond interactions. Two molecules of IMC orthogonally connected via C-H...O and C-H...N hydrogen bond interactions and such two pairs form a cube like motif Figure 6a and b. Such cubic motifs are propagated in all the directions Figure 6c.

3.8. Optical characterization

3.8.1. Absorption spectra

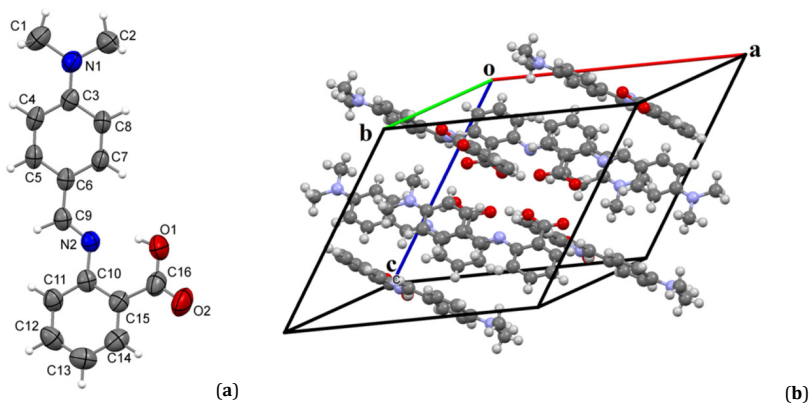
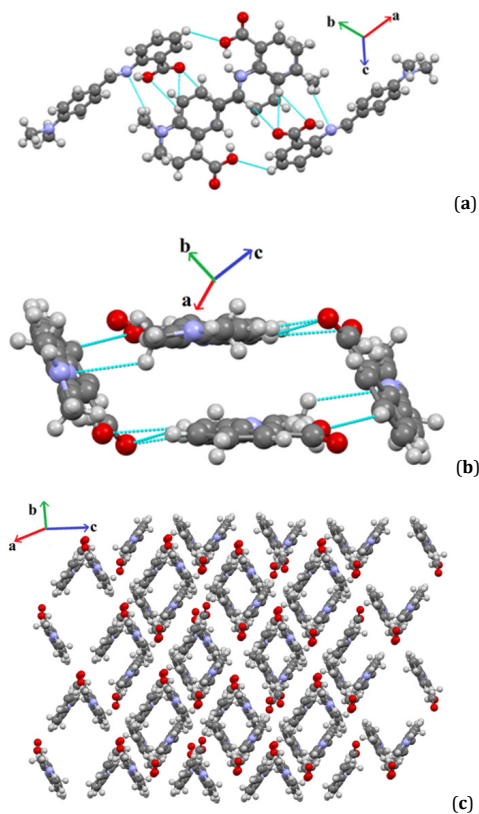
The absorption spectrum of AA shows three bands at 216, 249 and 335 nm ascribed to the $\sigma \rightarrow \pi^*$, $\pi \rightarrow \pi^*$ and $n \rightarrow \pi^*$ transitions, respectively, and DMAB also shows three bands at 204, 242 and 341 nm due to the $\sigma \rightarrow \pi^*$, $\pi \rightarrow \pi^*$ and $n \rightarrow \pi^*$ transitions, respectively [24], and the spectra are shown in Figure 7. The absorption spectra of the inter-molecular compound shows three bands same as AA but different intensities, and the λ_{\max} absorptions show hypo-chromic and hyper-chromic shift with respect to DMAB and AA, respectively.

3.8.2. Emission spectra

DMAB and AA show very low emission with λ_{\max} 380 and 405 nm upon their λ_{\max} excitation, respectively. The inter-molecular compound shows strong dual emission with two λ_{\max} one at 380 nm and the second at 450 nm (Stoke's shift 39 and 112 nm) upon excitation at 339 nm as shown in Figure 8. The total quantum efficiency of the IMC was found to be 0.49.

Table 5. Bond distances (Å) and angles (°) in the IMC.

C1- N1	1.458(3)	C6- C7	1.405(2)	C11- C12	1.372(3)
C2- N1	1.459(2)	C6- C9	1.431(3)	C12- C13	1.370(3)
C3- N1	1.368(2)	C7- C8	1.371(3)	C13- C14	1.381(3)
C3- C4	1.411(2)	C9- N2	1.280(2)	C14- C15	1.391(3)
C3- C8	1.407(2)	C10- N2	1.414(2)	C15- C16	1.502(2)
C4- C5	1.368(2)	C10- C11	1.399(2)	C16- O2	1.206(2)
C5- C6	1.397(3)	C10- C15	1.401(2)	C16- O1	1.314(2)
C1- N1- C2	116.35(17)	C7- C8- C3	121.33(16)	C11- C12- C13	121.09(19)
C1- N1- C3	121.63(17)	C5- C6- C9	120.53(16)	C12- C13- C14	119.4(2)
C2- N1- C3	121.41(17)	C7- C6- C9	123.14(18)	C13- C14- C15	120.9(2)
N1- C3- C8	121.37(16)	C6- C9- N2	124.28(16)	C14- C15- C10	119.44(17)
N1- C3- C4	121.42(17)	C9- N2- C10	123.65(15)	C14- C15- C16	117.03(19)
C8- C3- C4	117.20(18)	N2- C10- C15	117.03(15)	C10- C15- C16	123.48(18)
C3- C4- C5	120.41(17)	N2- C10- C11	124.27(17)	C15- C16- O2	121.2(2)
C4- C5- C6	122.95(16)	C15- C10- C11	118.69(17)	C15- C16- O1	117.27(19)
C5- C6- C7	116.33(18)	C10- C11- C12	120.46(19)	O2- C16- O1	121.44(19)
C6- C7- C8	121.76(18)				

**Figure 5.** (a) ORTEP representations of the asymmetric unit (50% ellipsoidal probability) (b) Unit cell diagram for IMC.**Figure 6.** (a) Hydrogen bonding pattern, (b) cubic motif and (c) three dimensional packing of IMC.

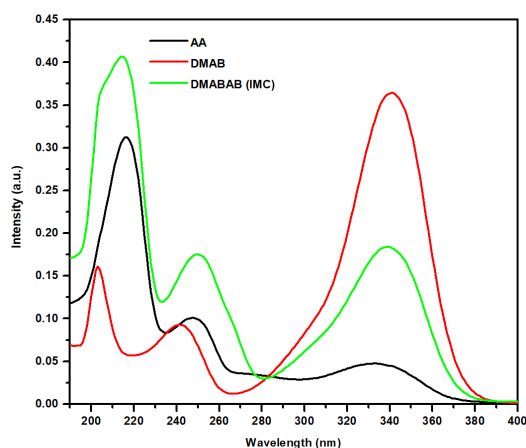


Figure 7. Absorption spectra of AA, DMAB and their IMC.

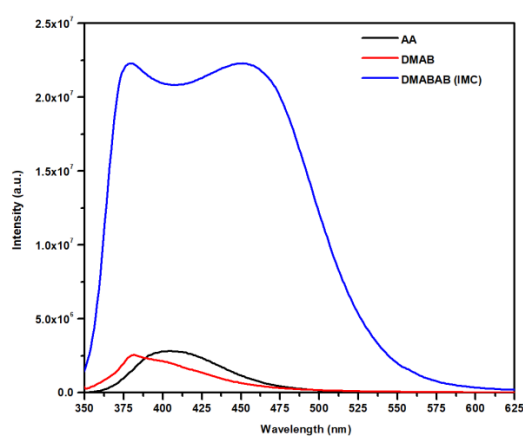


Figure 8. Emission spectra of AA, DMAB and their IMC.

4. Conclusions

The phase diagram study of AA-DMAB system shows the formation of 1:1 intermolecular compound with congruent melting point and two eutectics one on either side of the IMC. The heat of mixing is negative suggesting thereby a clustering of molecules for both binary eutectic melts. The powder X-ray diffraction patterns confirm the formation of an intermolecular compound that behaves as pure component for both the eutectics and thus is in accordance with the phase diagram. The values of heat of mixing are negative -0.36 and -4.17 kJ/mol for E_1 and E_2 , respectively, suggesting thereby a clustering of molecules in both the binary eutectic melts. The positive values of excess free energy for both eutectics (0.2013 and 0.4624 kJ/mol for E_1 and E_2 , respectively) indicate that the interaction between the like molecules are stronger than the interaction between the unlike molecule. From the single crystal X-ray analysis of IMC it can be inferred that it crystallizes in monoclinic unit cell with $C2/c$ space group, and reasonably large sized IMC crystal was grown by slow evaporation technique from methanol at room temperature. The IMC shows strong dual emission with two λ_{max} one at 380 nm and the second at 450 nm with total quantum efficiency of 0.49.

Acknowledgements

The one of authors (Dr. Manjeet Singh) would like to thank University Grand Commission for providing research fellowship.

Supporting information

CCDC-940623 contains the supplementary crystallographic data for this paper. These data can be obtained free of charge via <https://www.ccdc.cam.ac.uk/structures/>, or by e-mailing data_request@ccdc.cam.ac.uk, or by contacting The Cambridge Crystallographic Data Centre, 12 Union Road, Cambridge CB2 1EZ, UK; fax: +44(0)1223-336033.

Disclosure statement

Conflict of interests: The authors declare that they have no conflict of interest.
 Author contributions: All authors contributed equally to this work.
 Ethical approval: All ethical guidelines have been adhered.
 Sample availability: Samples of the compounds are available from the author.

ORCID

Uma Shanker Rai
 <http://orcid.org/0000-0002-3203-6820>
 Manjeet Singh
 <http://orcid.org/0000-0002-9081-2242>
 Rama Nand Rai
 <http://orcid.org/0000-0003-1681-5098>

Reference

- [1]. Rai, R. N.; Reddi, R. S. B.; Rai, U. S. *Prog. Cryst. Growth Charact. Mater.* **2013**, *59*, 73-11.
- [2]. Escher, C.; Winger, R. *Adv. Mater.* **1992**, *4*, 189-197.
- [3]. Ishiguro, T.; Yamaji, K.; *ET Salts: Quasi Two-Dimensional Systems, Organic superconductors*, Springer, Berlin Heidelberg, 1990.
- [4]. Miller, J. S. *Adv. Mater.* **1990**, *2*, 98-99.
- [5]. Rice, J. W.; Suuberg, E. M. *J. Chem. Therm.* **2010**, *42*, 1356-1360.
- [6]. Dwivedi, Y.; Kant, S.; Rai, S. B.; Rai, R. N. *J. Fluores.* **2011**, *21*, 1255-1263
- [7]. Dwivedi, Y.; Kant, S.; Rai, R. N.; Rai, S. B. *Appl. Phys. B* **2010**, *101*, 639-642.
- [8]. Henningsen, T.; Singh, N. B.; Hopkins, R. H.; Mazelsky, R.; Hopkins, F. K.; Frazier, D. O.; Singh, O. P. *Mater. Lett.* **1994**, *20*, 203-209.
- [9]. Rai, R. N.; Mudunuri, S. R.; Reddi, R. S. B.; Kumar Satuluri, V. S. A.; Ganeshmoorthy, S.; Gupta, P. K. *J. Cryst. Growth* **2011**, *321*, 72-77.
- [10]. Dean, J. A. *Lange's handbook of chemistry*, McGraw-Hill, New York, 1985.
- [11]. Singh, M.; Pandey, P.; Rai, R. N.; Rai, U. S. *J. Therm. Anal. Calorim.* **2013**, *113*, 977-983.
- [12]. Reddi, R. S. B.; Kant, S.; Rai, U. S.; Rai, R. N. *J. Cryst. Growth* **2009**, *312*, 95-99.
- [13]. Bruker. APEX2, SAINT, and SADABS; Bruker AXS Inc., Madison, Wisconsin, USA, 2011.
- [14]. Sheldrick, G. M. *Shelx-97, Program for Crystal Structure Refinement from Diffraction Data*, University of Gottingen, Gottingen, 1997.
- [15]. Rai, R. N.; Varma, K. B. R. *Mater. Lett.* **2000**, *44*, 284-293.
- [16]. Rai, R. N. *J. Mater. Res.* **2004**, *19*, 1348-1355.
- [17]. Singh, M.; Rai, R. N.; Rai, U. S. *Amer. J. Anal. Chem.* **2011**, *2*, 953-961.
- [18]. Rai, R. N.; Rai, U. S. *Thermochim. Acta* **2000**, *363*, 23-28.
- [19]. Christian, J. W. *The theory of phase transformation in metals and alloys*, Pergamon Press, Oxford, pp. 992, 1965.
- [20]. Singh, N.; Singh, N. B.; Rai, U. S.; Singh, O. P. *Thermochim. Acta* **1985**, *95*, 291-293.
- [21]. Kant, S.; Reddi, R. S. B.; Rai, R. N. *Fluid Phase Equilib.* **2010**, *29*, 171-175.
- [22]. Rai, R. N.; Varma, K. B. R. *Mater. Lett.* **2000**, *44*, 284-293.
- [23]. Singh, M.; Rai, R. N.; Rai, U. S. *J. Cryst. Growth* **2015**, *419*, 114-122.
- [24]. Kalsi, P. S. *Spectroscopy of Organic Compounds*, 6th Edition, New Age Publication, India, pp. 1-12, 2005.



Copyright © 2018 by Authors. This work is published and licensed by Atlanta Publishing House LLC, Atlanta, GA, USA. The full terms of this license are available at <http://www.eurjchem.com/index.php/eurjchem/pages/view/terms> and incorporate the Creative Commons Attribution-Non Commercial (CC BY NC) (International, v4.0) License (<http://creativecommons.org/licenses/by-nc/4.0>). By accessing the work, you hereby accept the Terms. This is an open access article distributed under the terms and conditions of the CC BY NC License, which permits unrestricted non-commercial use, distribution, and reproduction in any medium, provided the original work is properly cited without any further permission from Atlanta Publishing House LLC (European Journal of Chemistry). No use, distribution or reproduction is permitted which does not comply with these terms. Permissions for commercial use of this work beyond the scope of the License (<http://www.eurjchem.com/index.php/eurjchem/pages/view/terms>) are administered by Atlanta Publishing House LLC (European Journal of Chemistry).